

Two-step gap opening across the quantum critical point in a Kitaev honeycomb magnet

Yuya Nagai,¹ Takaaki Jin-no,² Junki Yoshitake,³ Joji Nasu,⁴ Yukitoshi Motome,³ Masayuki Itoh,¹ and Yasuhiro Shimizu¹

¹*Department of Physics, Graduate School of Science, Nagoya University, Furo-cho, Chikusa-ku, Nagoya 464-8602, Japan.*

²*Technical Center, Nagoya University, Furo-cho, Chikusa-ku, Nagoya 464-8601, Japan.*

³*Department of Applied Physics, University of Tokyo, Hongo, 7-3-1, Bunkyo, Tokyo 113-8656, Japan.*

⁴*Department of Physics, Tokyo Institute of Technology, Ookayama, 2-12-1, Meguro, Tokyo 152-8551, Japan.*

(Dated: October 15, 2018)

Quantum spin liquid involves fractionalized quasiparticles such as spinons and visons. They are expressed as itinerant Majorana fermions and Z_2 fluxes in the Kitaev model with bond-dependent exchange interactions on a honeycomb spin lattice¹. The observation has recently attracted attention for a candidate material α - RuCl_3 , showing spin liquid behaviour induced by a magnetic field²⁻¹³. Since the observable spin excitation is inherently composed of the two quasiparticles, which further admix each other by setting in the magnetic field as well as non-Kitaev interactions¹⁴⁻¹⁷, their individual identification remains challenging. Here we report an emergent low-lying spin excitation through nuclear magnetic and quadrupole resonance measurements down to ~ 0.4 K corresponding to 1/500 of the exchange energy under the finely tuned magnetic field across the quantum critical point. We determined the critical behaviour of low-lying excitations and found evolution of two kinds of the spin gap at high fields. The two excitations exhibit repulsive magnetic field dependence, suggesting anti-crossing due to the hybridization between fractionalized quasiparticles.

Quantum liquids involve quasiparticles following fractional statistics, as known in the fractional quantum Hall effect for charge degrees of freedom¹⁸. On Mott insulators, the spin excitation of quantum spin liquids without long-range ordering can be fractionalized into spinons and visons corresponding to itinerant Majorana fermions (MF) and localized Z_2 gauge fluxes for the soluble Kitaev model $\mathcal{H} = \sum_{(i,j)} \sum_{\gamma} J_K S_i^{\gamma} S_j^{\gamma}$, where J_K is the bond-dependent exchange coupling between two spins along directions $\gamma (= x, y, z)$ on the honeycomb lattice (Fig. 1a)^{1,19}. Although MF and Z_2 fluxes do not carry electric charges, they can display unique thermodynamics and spin dynamics. For example, they are individually excited at characteristic temperatures, $T_H \approx 0.375J_K$ and $T_L \approx 0.012J_K$, leading to a two-step entropy release²⁰. The MF excitation gives a gapless broad continuum up to the energy scale of J_K in the excitation spectrum. Despite a flux gap below $T_L \approx 0.012J_K$ (Ref. 14, 16, 21, and 22), the energy scale is usually too small to be identified in real materials because of long-range ordering at low temperatures.

A honeycomb-lattice magnet α - RuCl_3 attracts salient interests as an example of the Kitaev model²⁻⁴. The step-wise entropy release^{3,8,20} and the excitation continuum^{4,6,8,16} above the antiferromagnetic ordering temperature $T_N = 7-14$ K highlight the Kitaev physics. The spin liquid ground state appears as the in-plane magnetic field exceeds a critical value $H_c = 7-8$ T (Ref. 9-11, 13, and 23), above which the spin gap grows with increasing magnetic field^{9-12,23}. However, the field dependence of the spin excitation remains controversial; for experiments including the electron spin resonance spectroscopy¹² and the specific heat^{9,11}, the spin gap persists down to zero field or vanishes around H_c . Theoretically, the MF excitation becomes also gapped under the magnetic field¹ and constructs a non-trivial admixture with the flux excitation^{13,15}.

We investigate low-energy spin excitations via nuclear magnetic resonance (NMR) and nuclear quadrupole resonance (NQR) on α - RuCl_3 , which are complementary to high energy probes such as inelastic neutron scattering measure-

ments. The NMR Knight shift and nuclear spin-lattice relaxation rate T_1^{-1} measure the static spin susceptibility χ and the dynamical one $\chi(\mathbf{q}, \omega)$ with the wave vectors \mathbf{q} and the NMR frequency ω , respectively, which characterize fractional excitations of the Kitaev spin liquid at finite temperatures¹⁶ and an effect of non-Kitaev interactions^{13,15}. Previous NMR measurements conducted at high fields ($H > H_c$) and high temperatures ($T > 1.5$ K) uncovered the significant field dependence of T_1^{-1} , highlighting a possible spin liquid state. However, the detailed field evolution of quasiparticles is still in debate: e.g., the spin gap increases linearly above H_c (Ref. 10) or with a cubic law across H_c (Ref. 26), or is absent²⁵. For solving the discrepancy, we conducted comprehensive measurements including zero-field NQR and finely field-tuned NMR down to low temperatures (> 0.4 K) for observing the quasiparticles from the ground state.

First we show the result of ³⁵Cl and ³⁷Cl NQR in the absence of magnetic field (Fig. 1). A single NQR spectrum (Fig. 1b) for each nucleus ($I = 3/2$) with extremely sharp linewidth (~ 9 kHz) means a single Cl site in the crystal structure as expected for a rhombohedral $R\bar{3}$ lattice²⁷. The resonance frequency (16.89 MHz, 13.31 MHz) and the spectral intensity well scale to the electric quadrupole moment (³⁵ $Q = -8.2 \times 10^{-26}$, ³⁷ $Q = -6.5 \times 10^{-26}$ cm²) and the natural abundance (³⁵ $W = 75\%$, ³⁷ $W = 25\%$), respectively. Above 150 K, the spectrum splits into two with the intensity ratio of 2:1 (Fig. 1c), consistent with two Cl sites in the monoclinic $P2_1/c$ structure²⁷. The two phases coexist on the first-order structural transition around 120 K.

At zero field, T_1^{-1} measured for ³⁵Cl and ³⁷Cl (Fig. 1d) is independent of temperature T above 100 K, where the values for two nuclei scale to the square of the nuclear gyromagnetic ratio γ_n due to dominant magnetic fluctuations (Fig. S1). The similar behaviour was observed for ³⁵Cl NMR (Fig. 2). The constant value ($T_1^{-1} = 107$ s⁻¹ for $H||c$) yields an effective exchange coupling $J = 170$ K (Ref. 28, Supplementary Information), in agreement with the previous estimate^{8,26}. With decreasing T , T_1^{-1} starts to increase below 60 K. Instead

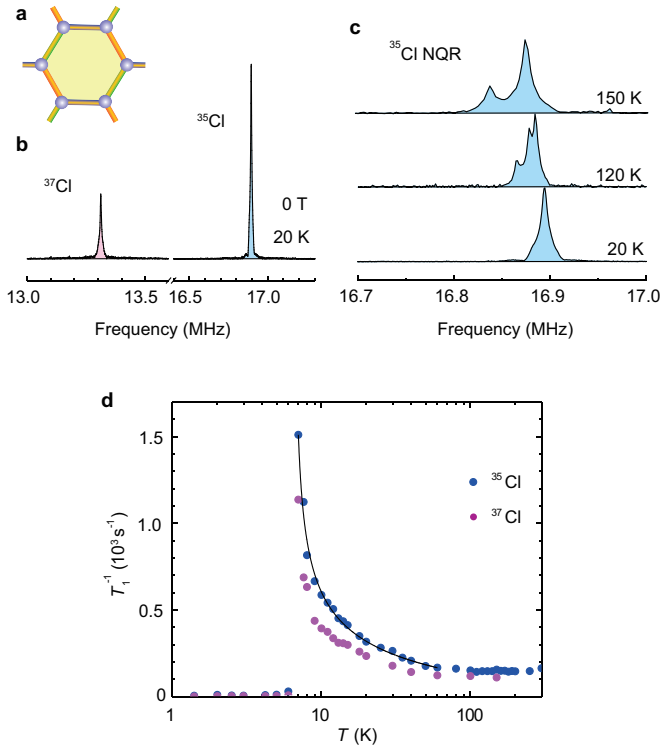


FIG. 1. **Zero-field NQR on a honeycomb magnet α - RuCl_3 .** **a**, Kitaev model with bond-dependent exchange interactions on the honeycomb lattice. **b**, ^{35}Cl and ^{37}Cl NQR spectra at 20 K. **c**, Temperature T dependence of ^{35}Cl NQR spectrum for cooling process across the structural phase transition around 120 K. **d**, Nuclear spin-lattice relaxation rate, T_1^{-1} , measured for ^{35}Cl and ^{37}Cl nuclei, which well scales to the square of the nuclear gyromagnetic ratio, γ_n^2 (see also Fig. S1). Solid curve: a fitting result by a scaling function $T_1^{-1} \sim (T/T_N - 1)^{z'}$ with $T_N = 6.5 \pm 0.2$ K and the critical exponent $z' = 0.45 \pm 0.03$.

of the broad peak of T_1^{-1} as expected in the Kitaev model¹⁶, we observed a divergent enhancement with a scaling form $T_1^{-1} \sim (T/T_N - 1)^{z'}$ toward $T_N = 6.5$ K. The critical exponent $z' = 0.45 \pm 0.02$ is distinct from that of the two-dimensional Ising antiferromagnet ($z' = 0.75$)^{29,30}. Therefore, T_1^{-1} just above T_N is likely governed by spin fluctuations at a finite wave vector ($q \neq 0$) toward magnetic ordering.

Under the magnetic field of 9.0 T, we measured the ^{35}Cl Knight shift, K_c and K_{b^*} , for the out-of-plane c axis and the in-plane b^* axis normal to the a axis, which displays highly anisotropic behaviour (Fig. 2a). Here we evaluated the Knight shift by simulating the NMR spectrum using the nuclear quadrupole frequency ν_Q obtained from the NQR measurement (Figs. S2–S4). We find that K_c is independent of T , while K_{b^*} is largely enhanced at low temperatures ($T \lesssim T_H = 60$ K), as observed in the bulk magnetic susceptibility χ , and then it levels off below $T^* \sim 10$ K $\approx 0.06J$. Instead of the magnetic ordering, K_{b^*} shows a broad maximum around 4 K and becomes T -independent for $T \lesssim T_L = 2$ K without an indication of magnetic ordering down to 0.4 K ($\approx 0.002J_K$). In comparison with the numerical calculation^{16,21,22}, the constant

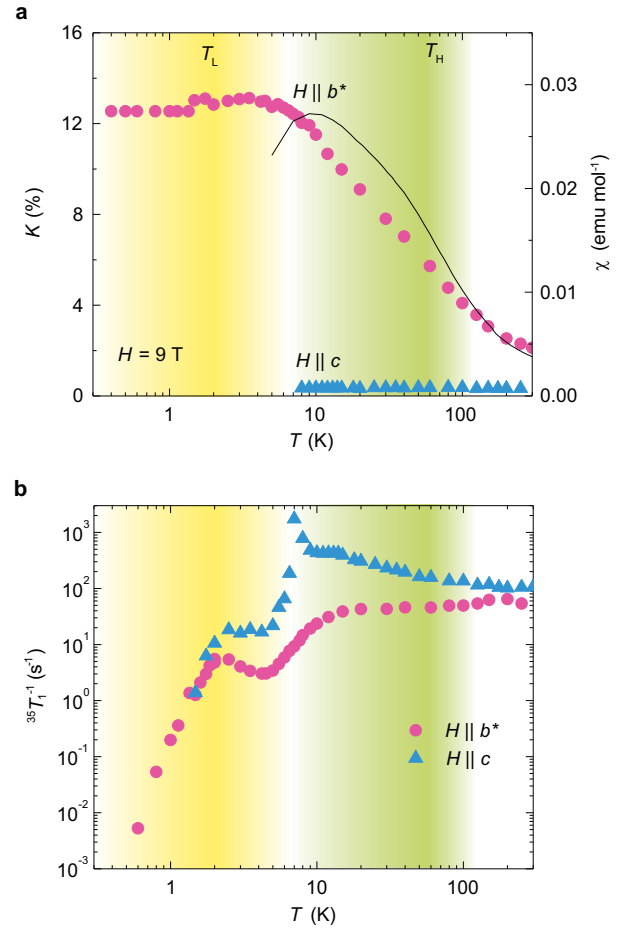


FIG. 2. **Anisotropic static and dynamical spin susceptibility.** **a**, Temperature dependence of Knight shifts K_c and K_{b^*} at 9 T applied parallel and perpendicular to the c axis, in comparison with the magnetic susceptibility χ (solid curve, the right-hand axis) at 1.0 T applied along the ab plane. **b**, Nuclear spin-lattice relaxation rate T_1^{-1} for $H \parallel c$ and b^* , which measures the dynamical spin susceptibility normal to the field, $\chi_{\perp}(\mathbf{q}, \omega)$. T_H and T_L denote the temperatures where MF and Z_2 fluxes are thermally excited, respectively¹⁶.

$K_{b^*} = 12.5\%$ corresponding to 0.028 emu mol⁻¹ is located in between antiferromagnetic (0.0058 emu mol⁻¹) and ferromagnetic (0.093 emu mol⁻¹) cases, indicating the significant ferromagnetic spin correlation.

The T dependence of T_1^{-1} is also highly anisotropic, as shown in Fig. 2b. In general, T_1^{-1} monitors spin fluctuations with wave vectors \mathbf{q} normal to the external field. In the present case, owing to the strong easy-plane anisotropy, in-plane spin fluctuations dominate T_1^{-1} for both $H \parallel c$ and b^* , and hence the observed anisotropy of T_1^{-1} should come from the dependence of spin excitations against the in-plane field component. Indeed, for $H \parallel c$ without the in-plane component, T_1^{-1} exhibits similar behaviour to that of zero field, showing a sharp peak at $T_N = 6.5$ K. For $H \parallel b^*$, T_1^{-1} is nearly independent of T down to 20 K and then becomes suppressed, pointing to a gap opening over the \mathbf{q} space. Upon further cooling, a prominent

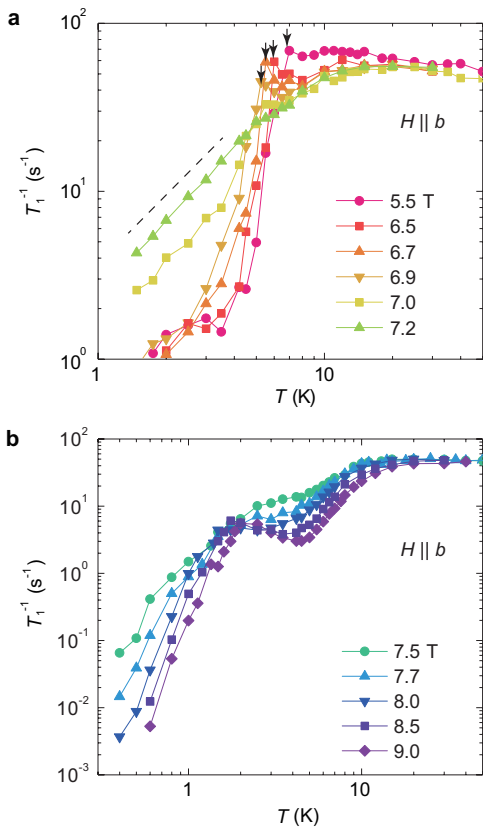


FIG. 3. **Nuclear spin-lattice relaxation rate T_1^{-1} under finely tuned magnetic field.** Temperature dependence of T_1^{-1} (a) in a low field range below 7.2 T and (b) a high field range above 7.5 T. A sharp peak is observed at the magnetic ordering temperature T_N marked by arrows, below which T_1^{-1} decreases exponentially. Around H_c , T_1^{-1} obeys the $T^{3/2}$ dependence represented as the dotted line.

peak appears around T_L , followed by a steep suppression. The result signifies that there are two kinds of the spin gap in the excitation spectrum of the field-driven spin liquid state.

The in-plane magnetic field dependence of T_1^{-1} is investigated in details around the critical field H_c , as shown in Fig. 3. In a low field range (Fig. 3a), T_1^{-1} exhibits a broad maximum around 15–20 K, which is shifted to higher temperatures with increasing H . The T dependence is distinct from conventional antiferromagnets showing a power-law evolution toward T_N but similar to the behaviour expected for the Kitaev model where the spin gap opens in the ground state¹. Above T_N , we evaluate the spin gap by fitting T_1^{-1} into an extended exponential function $T_1^{-1} \propto T^{-n} e^{(-\Delta_H/T)}$ ($n = 1$, Fig. 4a) for $10 < T < 30$ K (Ref. 26). The obtained gap Δ_H obeys a relation $\Delta_H \sim \Delta_0 + bH^\delta$ with the power $\delta = 3.0 \pm 0.3$ for $H > 5.5$ T (Fig. 4b) in agreement with the Kitaev’s prediction¹ showing H^3 dependence of the MF gap. An extrapolation to zero field yields a constant value $\Delta_0 = 7 \pm 1$ K, close to the flux gap $0.065J_K \sim 10$ K (Ref. 1) and Δ_0 estimated from the angular dependence of T_1^{-1} (Ref. 26).

In the magnetically ordered state, we observed a steep T_1^{-1} drop due to gapped spin-wave excitations in presence of the

strong magnetic anisotropy. We evaluated the magnon gap Δ_m based on the three-magnon process with $T_1^{-1} = AT^2 e^{(-\Delta_m/T)}$ (Fig. S4)³¹. The obtained $\Delta_m = 60$ K at zero field is suppressed toward $H'_c = 7.10 \pm 0.02$ T (Fig. 4b) following $\Delta_m \propto (1 - H/H'_c)^{2\nu}$ ($\nu = 0.36 \pm 0.03$). Here H'_c is slightly lower than $H_c = 7.40$ T for T_N (Fig. 4c, Fig. S7), as obtained from the T and H dependence of T_1^{-1} . The vanishing magnon gap below H_c indicates emergence of a gapless magnetic phase with strong spin fluctuations, where T_1^{-1} obeys a power law $T_1^{-1} \sim T^n$ ($n \sim 1.5$). As Δ_H overcomes Δ_m around 7 T, the spin liquid state persists down to low temperatures. At $H = 7.5$ T just above H_c , we still find power-law T dependence of T_1^{-1} ($n \sim 2$) below 4 K, implying a linear Dirac dispersion with a tiny gap down to low energies.

For $H > H_c$, T_1^{-1} continues to be suppressed, and a prominent peak around 1–2 K is shifted to higher temperatures (Fig. 3b). Thus, a lower-lying gap also increases with H . We can evaluate the spin gap Δ_L using the same equation as for Δ_H below 4 K (Fig. 4a). As shown in Fig. 4b, Δ_L is suppressed toward H_c . The origin of Δ_L is unlikely attributed to a forced ferromagnetic state, because there is no indication of the saturated magnetization in the K measurements below 9 T (Fig. S7). The peak structure of T_1^{-1} around 2 K indicates a sizable spectral weight above Δ_L (~ 0.2 – 0.5 meV). The energy scale of Δ_L is lower than the spin gap at $q = 0$ as observed in the electron spin resonance^{11–13}.

The quantum criticality of low-lying excitations is visualized by plotting $(T_1 T)^{-1}$ as a function of T and H in the contour plot (Fig. 4c, Fig. S8). In quantum critical magnets, $(T_1 T)^{-1}$ or the dynamical spin susceptibility $\chi(\mathbf{q}, \omega)$ would be divergently enhanced for $T \rightarrow 0$ at H_c , as the spin correlation length ξ grows with a power law, $\xi \sim T^{-\nu}$ ($\nu = 1$ for two-dimensional Ising magnets). Since $(T_1 T)^{-1}$ relates to ξ with $(T_1 T)^{-1} \propto \xi^{z-\eta}$ based on the dynamical scaling hypothesis^{29,32}, the absence of the critical enhancement in $(T_1 T)^{-1}$ shows that the spin correlation remains finite due to the development of Δ_H over the \mathbf{q} space.

In the Kitaev model, the spin excitation is expressed with a composite of the gapless MF and the gapped fluxes, resulting in the nonzero spin gap from the ground state to the excited states at zero field. When the magnetic field is introduced, the MF excitation is also gapped, and furthermore the two excitations are not defined independently and entangled with each other. Thus, it is natural to observe two spin gaps in the presence of the magnetic field. In addition, an anti-crossing between the two excitations is expected to occur at some field, as the perturbation theory suggests less H dependence of the flux gap and a rapid increase of the MF gap proportional to H^3 (Ref. 1). Interestingly, as shown in Fig. 4b, Δ_H , which originally reflects the flux character at $H \rightarrow 0$, has a concave H dependence, while Δ_L is convex. This appears to be consistent with the anticipated anti-crossing behaviour. In this scenario, Δ_L is ascribed to the excitation that originally reflects the MF character but gradually acquires the flux character while increasing H (see Fig. 4d). Thus, our observation of the two-step gap opening would be a direct evidence of the two-types of entangled excitations, although it is obviously necessary to clarify the effect of non-Kitaev interactions for complete un-

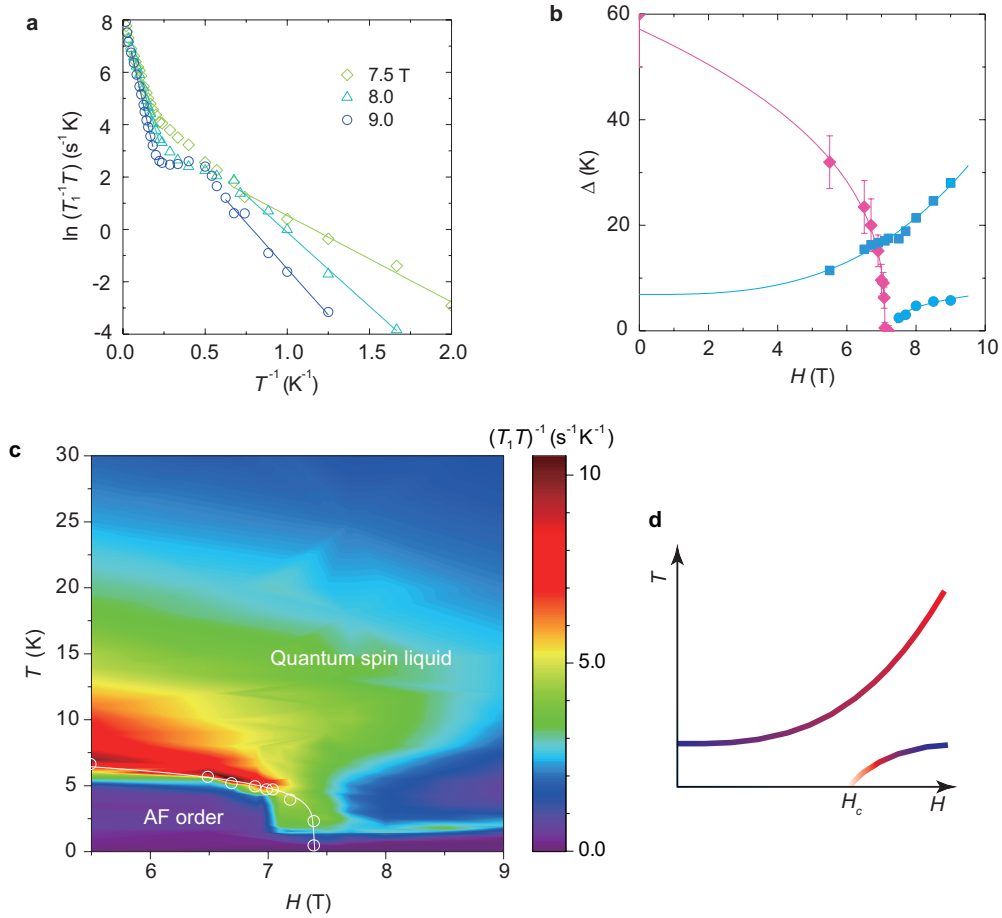


FIG. 4. **Criticality of low-lying spin excitations.** **a**, Inverse temperature dependence of $\ln(TT_1^{-1})$. The slopes yield the spin gap, Δ_H and Δ_L , for temperature ranges, 7 – 20 K and 0.5 – 4 K, respectively. **b**, Magnetic field dependence of the magnon gap Δ_m (red diamond), Δ_H (blue square), and Δ_L (blue circle). **c**, Contour plot of $(T_1 T)^{-1}$ as a function of magnetic field H and temperature T . Circles denote T_N defined by the T_1^{-1} peak against H and T . A solid curve is a fitting result with $T_N \sim (1 - H/H_c)^\nu$, yielding $H_c = 7.40 \pm 0.03$ T and the critical exponent $\nu = 0.22 \pm 0.02$. **d**, Schematic energy diagram of fractionalized gapped excitations. The dominant Majorana and gauge flux contributions are colored with red and blue, respectively.

derstanding, including the critical behavior at H_c .

Our observations of the local spin susceptibility and low-energy spin dynamics demonstrate the two types of spin excitations in the field-driven quantum spin liquid state. It strongly suggests the emergent entanglement between the fractionized MF and Z_2 fluxes under the magnetic field. The recombination process and the quantum criticality are the intriguing future issue requiring further extensive investigations beyond the analytically soluble Kitaev model.

Crystal growth and characterization Single crystals of α -RuCl₃ were grown by a sublimation method. The starting material of anhydrous ruthenium trichloride was dried in vacuum at 250 °C for 24 hours. The powder sealed in a quartz tube was heated up to 1100 °C and slowly cooled down to 600 °C under the spacial thermal gradient. The plate crystals were obtained in the cooler side of the tube. Since the crystal might cause metastable stacking faults by applying stress, we took special care for handing the crystal. The quality of the single crystal was evaluated by measuring x-ray diffraction, NMR, NQR,

and magnetic susceptibility. The magnetization was measured with a superconducting quantum interference device (SQUID) magnetometer (MPMS-XS, Quantum Design Ltd.) at 1 T. The magnetic transition was observed only at $T_N = 6.5$ K in magnetic susceptibility and NQR measurements, signifying a single domain crystal without a stacking fault.

Nuclear quadrupole and magnetic resonance We performed ³⁵Cl and ³⁷Cl NQR measurements on a single crystal at zero field down to 1.4 K. NMR was measured at constant magnetic fields up to 9.0 T in a temperature range of 0.4–300 K by utilizing a ³He cryostat below 1.5 K. The NQR and NMR spectra were obtained from Fourier transformation of temporal spin-echo evolution after $\pi/2$ and π pulses with an interval time $\tau = 40 \mu\text{s}$. The nuclear spin-lattice relaxation rate T_1^{-1} was obtained from a nuclear magnetization recovery fitted to an exponential function $\frac{M(\infty)-M(t)}{M(\infty)} = 0.1e^{-t/T_1} + 0.9e^{-6t/T_1}$ for the central NMR line or fitted to a stretched exponential function below 10 K. The spin-echo decay rate T_2^{-1} was obtained from the 2τ dependence of the integrated spin-echo

intensity. Beyond the second-order approximation of electric quadrupole contribution to the spectral shift, the ^{35}Cl Knight shift was evaluated by analyzing the central line position with the exact diagonalization of the nuclear spin Hamiltonian $\mathcal{H} = \mathbf{S} \cdot \mathbf{A} \cdot \mathbf{I} + \mathbf{I} \cdot \mathbf{q} \cdot \mathbf{I}$ for the electron spin \mathbf{S} , the hyperfine

coupling tensor \mathbf{A} , and the electric quadrupole coupling tensor \mathbf{q} by considering the temperature dependence of the NQR frequency (Fig. S1). Further details of the spectral assignment were described in Supplementary Information.

- ¹ Kitaev, A. Anyons in an exactly solved model and beyond. *Ann. Phys. (Amsterdam)* **321**, 2–111 (2006).
- ² Plumb, K. W. *et al.* α - RuCl_3 : A spin-orbit assisted Mott insulator on a honeycomb lattice. *Phys. Rev. B* **90**, 041112 (2014).
- ³ Kubota, Y. *et al.* Successive magnetic phase transitions in α - RuCl_3 : XY-like frustrated magnet on the honeycomb lattice. *Phys. Rev. B* **91**, 094422 (2015).
- ⁴ Sandilands, L. J., Tian, Y., Plumb, K. W., & Kim, Y.-J. Scattering continuum and possible fractionalized excitations in α - RuCl_3 . *Phys. Rev. Lett.* **114**, 147201 (2015).
- ⁵ Chaloupka, J. & Khaliullin, G. Magnetic anisotropy in the Kitaev model systems Na_2IrO_3 and RuCl_3 . *Phys. Rev. B* **94**, 064435 (2016).
- ⁶ Banerjee, A. *et al.* Proximate Kitaev quantum spin liquid behaviour in a honeycomb magnet. *Nat. Mater.* **15**, 733–740 (2016).
- ⁷ Banerjee, A. *et al.* Neutron scattering in the proximate quantum spin liquid α - RuCl_3 . *Science* **356**, 1055–1059 (2017).
- ⁸ Do, S.-H. *et al.* Majorana fermions in the Kitaev quantum spin system α - RuCl_3 . *Nat. Phys.* **13**, 1079–1084 (2017).
- ⁹ Wolter, A. U. B. *et al.* Field-induced quantum criticality in the Kitaev system α - RuCl_3 . *Phys. Rev. B* **96**, 041405 (2017).
- ¹⁰ Baek, S.-H. *et al.* Evidence for a field-induced quantum spin liquid in α - RuCl_3 . *Phys. Rev. Lett.* **119**, 037201 (2017).
- ¹¹ Sears, J. A. *et al.* Phase diagram of α - RuCl_3 in an in-plane magnetic field. *Phys. Rev. B* **95**, 180411(R) (2017).
- ¹² Ponomaryov, A. N. *et al.* Unconventional spin dynamics in the honeycomb-lattice material α - RuCl_3 : High-field electron spin resonance studies. *Phys. Rev. B* **96**, 241107(R) (2017).
- ¹³ Winter, S. M. *et al.* Probing α - RuCl_3 beyond magnetic order: effects of temperature and magnetic field. *Phys. Rev. Lett.* **120**, 077203 (2018).
- ¹⁴ Knolle, J., Kovrizhin, D. L., Chalker, J. T. & Moessner, R. Dynamics of a two-dimensional quantum spin liquid: signatures of emergent Majorana fermions and fluxes. *Phys. Rev. Lett.* **112**, 207203 (2014).
- ¹⁵ Song, X. Y., You, Y. Z., & Balents, L. Low-energy spin dynamics of the honeycomb spin liquid beyond the Kitaev limit. *Phys. Rev. Lett.* **117**, 037209 (2016).
- ¹⁶ Yoshitake, J., Nasu, J. & Motome, Y. Fractional spin fluctuations as a precursor of quantum spin liquids: Majorana dynamical mean-field study for the Kitaev model. *Phys. Rev. Lett.* **117**, 157203 (2016).
- ¹⁷ Gohlke, M., Verresen, R., Moessner, R., & Pollmann, F. Dynamics of the Kitaev-Heisenberg model. *Phys. Rev. Lett.* **119**, 157203 (2017).
- ¹⁸ Laughlin, R. B. Anomalous quantum Hall effect: an incompressible quantum fluid with fractionally charged excitations. *Phys. Rev. Lett.* **50**, 1395–1398 (1983).
- ¹⁹ Jackeli, G. & Khaliullin, G. Mott insulators in the strong spin-orbit coupling limit: from Heisenberg to a quantum compass and Kitaev models. *Phys. Rev. Lett.* **102**, 017205 (2009).
- ²⁰ Nasu, J., Udagawa, M. & Motome, Y. Thermal fractionalization of quantum spins in a Kitaev model: Temperature-linear specific heat and coherent transport of Majorana fermions. *Phys. Rev. B* **92**, 115122 (2015).
- ²¹ Yoshitake, J., Nasu, J. & Motome, Y. Majorana dynamical mean-field study of spin dynamics at finite temperatures in the honeycomb Kitaev model. *Phys. Rev. B* **96**, 024438 (2017).
- ²² Yoshitake, J., Nasu, J. & Motome, Y. Temperature evolution of spin dynamics in two- and three-dimensional Kitaev models: Influence of fluctuating Z_2 flux. *Phys. Rev. B* **96**, 064433 (2017).
- ²³ Wang, Z. Magnetic excitations and continuum of a possibly field-induced quantum spin liquid in α - RuCl_3 . *Phys. Rev. Lett.* **119**, 227202 (2017).
- ²⁴ Wellm, C. *et al.* Signatures of low-energy fractionalized excitations in α - RuCl_3 from field-dependent microwave absorption, arXiv:1710.00670v.
- ²⁵ Zheng, J. Gapless spin excitations in the field-induced quantum spin liquid phase of α - RuCl_3 . *Phys. Rev. Lett.* **119**, 227208 (2017).
- ²⁶ Jansa, N. *et al.* Observation of gapped anyons in the Kitaev honeycomb magnet under a magnetic field. *Nat. Phys.* **14**, 786–790 (2018).
- ²⁷ Morosin, B. & Narath, A. X-ray diffraction and nuclear quadrupole resonance studies of chromium trichloride. *J. Chem. Phys.* **40**, 1958 (1964).
- ²⁸ Moriya, T. Nuclear magnetic relaxation in antiferromagnetics. *Prog. Theo. Phys.* **16**, 23–44 (1956).
- ²⁹ Hohenberg, P. C. & Halperin, P. I. Theory of dynamic critical phenomena. *Rev. Mod. Phys.* **49**, 435–479 (1977).
- ³⁰ Dutta, A. *et al.* *Quantum Phase Transitions in Transverse Field Spin Models: From Statistical Physics to Quantum Information* (Cambridge University Press, Cambridge, 2015).
- ³¹ Narath, A. & Fromhold, A. T. Nuclear spin-lattice relaxation of ^{53}Cr in the ordered magnetic insulator CrCl_3 . *Phys. Rev. Lett.* **17**, 354 (1966).
- ³² Sachdev, S. *Quantum Phase Transitions*, 2nd. Ed. (Cambridge Univ. Press. London, 2011).